Published in final edited form as:
Int J Hyperthermia. 2009 ; 25(6): 405–415. doi:10.1080/02656730903022700.

DCE-MRI Parameters Have Potential to Predict Response of Locally Advanced Breast Cancer Patients to Neoadjuvant Chemotherapy and Hyperthermia: A Pilot Study

Oana I. Craciunescu[1], **Kimberly L. Blackwell**[1], **Ellen L. Jones**[1], **James R. MacFall**[1], **Daohai Yu**[3], **Zeljko Vujaskovic**[1], **Terence Z. Wong**[1], **Vlayka Liotcheva**[1], **Eric L. Rosen**[2], **Leonard R. Prosnitz**[1], **Thaddeus V. Samulski**[1], and **Mark W. Dewhirst**[1]

[1]Duke University Medical Center, Durham, NC, USA

[2]University of Washington, Seattle, WA, USA

[3]Moffitt Cancer Center and Research Institute, FL, USA

Abstract

Purpose—To use a novel Morpho-Physiological Tumor Score (MPTS) generated from dynamic contrast-enhanced magnetic resonance imaging (DCE-MRI) to predict response to treatment.

Materials and Methods—A protocol was designed to acquire DCE-MRI images of 20 locally advanced breast cancer (LABC) patients treated with neoadjuvant chemotherapy (NA ChT) and hyperthermia (HT). Imaging was done over 30 minutes following bolus injection of Gd-based contrast agent. Parametric maps were generated by fitting the signal intensity to a double exponential curve and were used to derive a morphological characterization of the lesions. Enhancement-variance dynamics parameters, washin and washout parameters (WiP, WoP) were extracted. The morphological characterization and the WiP and WoP were combined into a MPTS with the intent of achieving better prognostic efficacy. The MPTS was correlated with response to NA therapy as determined by pathologic residual tumor and MRI imaging.

Results—The contrast agent in all tumors typically peaked in the first 1–4 minutes. The tumors WiP and WoP varied considerably. The MPTS was highly correlated with whether the patients had a pathologic response. This scoring system has a specificity of 78% and a sensitivity of 91% for predicting response to NA chemotherapy. The kappa was 0.69 with a 95% confidence interval of [0.38, 1.0] and a p-value of 0.002.

Conclusions—This pilot study shows that the MPTS derived using pre-treatment MRI images has the potential to predict response to NA ChT and HT in LABC patients. Further prospective studies are needed to confirm the validity of these results.

Keywords

neoadjuvant therapy; locally advanced breast cancer; hyperthermia; MR prognostic factors; magnetic resonance imaging

Corresponding author: Oana Craciunescu, PhD, DABR, Box 3295 Duke University Medical Center, Durham, NC, 27710, oana.craciunescu@duke.edu, Tel: (919) 660-2192.

1. Introduction

Locally advanced breast carcinoma comprises approximately 5–10% of all new breast carcinomas presenting in the United States (1). Three and five year disease-free survival in the setting of aggressive combined multimodality therapy is 65% and 55%, respectively (1,2). Given this poor prognosis, the optimal timing and sequencing of chemotherapy (ChT) and radiotherapy in relation to surgery have yet to be determined. Even with the most aggressive multimodality therapies, the complete pathological response rate after neoadjuvant therapy remains between 9–13%. In addition, the risk of developing distant metastases remains quite high and significant improvements in treatment needs to be made.

For women treated with neoadjuvant chemotherapy for locally advanced breast cancer (LABC), early determination of whether the patient will fail to respond can enable the use of alternative therapies that can be more beneficial. This goal can be potentially achieved using magnetic resonance imaging (MRI) with contrast enhancement using gadopentetate dimeglumine (Gd-DTPA) (3,4). DCE-MRI involves the intravenous bolus injection of a low-molecular weight contrast agent followed by a fast sequence image acquisition to measure the signal enhancement over time as the contrast agent travels through the tumor vasculature.

MRI of the breast is a sensitive method for noninvasively assessing both tumor morphology and physiology. Thus, breast MRI helps improve local staging, possibly predicts tumor vascularity, and potentially provides a unique noninvasive method for monitoring response to pre-surgical chemotherapy regimens (5). It has been shown that MR has the capability to extract parameters that can predict tumor physiology, response to neoadjuvant therapies, and patient outcome (4). DCE-MRI exploits tumor neovascularization. The contrast agent preferentially accumulates in tumor due to increased tumor perfusion and due to the increased permeability of tumor vasculature. Early accumulation of contrast agent likely reflects increased or altered vascularity relative to normal tissue (6). Correlative work in human trials has shown that the signal intensity, i.e. the increase in signal after the contrast agent (CA) arrival, relates to the vascular density of a lesion and that the rate of enhancement characterizes the vascular fenestration and functional permeability (7). The interstitial environment influences the diffusibility and temporary retention (wash-out) of the contrast agent (8).

Techniques of extracting MR parameters from DCE-MRI sequences are abundant in the radiology literature, where the analysis of the CA enhancement curves (intensity enhancement over time) has been proposed as a diagnostic tool in differentiating malignant versus benign lesions (6,9–13). Qualitatively, the kinetic curves were classified according to their shape in 3 types: type I - persistent enhancing, type II - plateau and type III -washout. It is accepted now that persistent curves are associated with benign disease, and washout curves with cancer (14). Figure 1 shows the three types of enhancement, with two different trends shown for the washout types (Figure 1C), both of which are encountered in LABC patients.

The first part of the enhancement curve reflects the rapid CA uptake by the tumor, and it is known as the early enhancement curve, or washin. The slope of the late enhancement (or washout) is related to the rate at which the CA is returned back to the blood pool. Tumor washout will vary significantly due to a large range of physiological factors including regional blood flow, endothelial permeability, the size and distribution of the extravascular extracellular space, and cellular fraction. A lesion with an enhancement curve like the dotted one in Figure 1C can have an initial high contrast but does not have a large extracellular space for the CA to distribute. In this way, the washout can be a surrogate for tumor extracellular extravascular space.

Signal enhancement assessment methods are either semi-quantitative (or non-model based) which analyze signal intensity changes (15,16), or quantitative (model-based) which directly

measure the change in concentration of the contrast agent using pharmacokinetic (PK) models . The most widely used quantitative method is the Tofts and Kermode model which uses a compartmental model to describe the exchange between the main blood compartment, whole body extracellular space, and lesion leakage space using an iterative fitting of a model function with parameters based on known physiological processes (17).

Using any of the above mentioned techniques of extracting MR parameters, several studies have examined the ability of DCE-MRI to predict or monitor breast cancer treatment response. Several authors explored the potential of DCE-MRI to evaluate response to NA chemotherapy for LABC patients (3) (18–22). Szabo et al., used MR-extracted parameters as prognostic factors in the same setting using data from 61 women with invasive breast cancer (23). They showed that the presence of a rim enhancement pattern, early maximal enhancement and washout phenomena are independently associated with establishing “predictors of poor prognosis (higher histologic grade, positive Ki-67, an immunohistochemically detected biomarker of proliferation, and negative estrogen receptor status)”. Pharmacokinetic analysis was used by Chang et al. (24) to estimate angiogenic response of LABC patients to NA chemotherapy. They noticed that tumors with better response tended to alter their internal composition from heterogeneous to homogeneous distribution and decrease in peak enhancement after chemotherapy. Wedam et al. (25) used MR extracted parameters to assess the antiangiogenic and antitumoral effects of bevacizumab in inflammatory LABC patients. The MR derived pharmacokinetic parameters (inflow transfer rate constant, extracellullar volume fraction) decreased after bevacizumab alone. In a more recent study, Padhani et al. (26) also looked at the ability of DCE-MRI to predict clinicopathological response. They showed that “transfer constant and size changes are equally sensitive in the identification of patients who would gain no clinical or pathological benefit after two cycles of treatment”. Another recent study by Manton et al. (27) looked at early response prediction with quantitative MR imaging and spectroscopy in LABC patients.

However, none of the above mentioned studies tried to predict response to treatment based on the pre-treatment MR data alone. In this study, given the importance of tumor morphology and physiology in the ultimate response to treatment, MR derived parameters were for the first time combined into a Morpho-Physiological Tumor Score (MPTS) with the intent of achieving a synergistic increase in prognostic efficacy in a group of LABC patients treated with NA chemotherapy and hyperthermia.

2. Materials and Methods

2.1 Clinical Protocol: NA + HT Therapy

At Duke University Medical Center, LABC patients were treated between 2000 and 2004 on an IRB approved Phase I/II clinical trial using a combination of Paclitaxel (Taxol, Bristol-Myers Squibb, Prinston, NJ), liposomal doxorubicin (Myocet, Elan Pharmaceuticals, Princeton, NJ) and HT every 21 days, for a total of four cycles, followed by surgery (see Figure 2 for protocol schema). All patients considered in this study were given the maximum tolerated dose established during the Phase I portion of the trial: 175 mg/m^2 for Paclitaxel and 75 mg/m^2 for liposomal doxorubicin.

2.2 HT Treatments

In this study the objective was to use HT to enhance the NA therapy. Four HT treatments were given every 21 days as part of neoadjuvant local and systemic therapy. Hyperthermia treatment started within an hour after chemotherapy was administered and lasted from 60 to 70 minutes. A catheter was pre-placed under CT guidance into the tumor to allow the insertion of a fiberoptic probe (Luxtron Corp., Santa Clara, CA) that mapped temperatures inside the breast

every 0.5 cm. Typically, anywhere between 5 and 10 cm of breast tissue was mapped depending on the tumor and breast size. Three additional probes were placed on the skin for temperature monitoring. Patients were heated prone in the Duke Breast Applicator System (DBAS) (28), with the involved breast hanging in a water-filled cup that provided electromagnetic coupling and surface temperature control. The four channels of the DBAS were independently adjusted for phase and amplitude during treatment to achieve desired steering and to optimize patient comfort. Operating frequencies ranged between 140 MHz and 156 MHz, depending on the cup used and the breast size, with power levels from 60 to 200W depending mainly on the patient threshold to pain. Maximum allowable temperatures in adjacent normal tissues and tumor were 43°C and 48°C, respectively., For the purpose of this analysis, only the CEM43T90 (cumulative equivalent minutes at 43°C (29), and T90 the temperature exceeded by 90% of the measured points) will be reported.

2.3 MR Imaging and Parameters

DCE-MRI was used to evaluate patients for clinical response. Scans were performed prior to each of the first two cycles of chemotherapy and at the completion of the preoperative therapy. Figure 2 shows a simplified schema of the time line that includes the 4 cycles of NA ChT (grey arrows) followed by surgery (bold arrow) and MRI sessions (filled arrows). Data reported in this study is based only on the pretheraphy DCE-MRI study, circled in Figure 2.

All MRI examinations were performed on a commercially available 1.5-T system (Signa, GE Healthcare, Milwaukee, WI) using a dedicated breast coil (Liberty 5000, USA Instruments, Aurora, OH), imaging only one breast. After an axial localizer image was obtained, a sagittally oriented fat-suppressed fast spin-echo (FSE) T2-weighted sequence was performed (TR/ TE, 4,000/110 msec; echo train length of 16, 512 × 512 matrix, FOV varied from 16 × 16 to 20 × 20 cm^2, depending on the brest size, 4.0 mm slice thickness; no gap). This sequence was followed by a 3D T1-weighted fat-suppressed gradient-recalled echo sequence (3D FGRE) with TR/TE, 5.5/1.5 msec, flip angle = 30°, and same FOV and slice thickness as the FSE scan. The sequence was reviewed before contrast administration to ensure adequate and uniform fat saturation. Then, gadopentetate dimeglumine (Gd-DTPA) (Magnevist [0.1 mmol per kilogram of body weight], Berlex, Wayne, NJ) was administered by a rapid injector through an indwelling IV catheter at a rate of 2 cm^3/sec. Contrast-enhanced imaging was initiated immediately after the CA was completely injected. Volume acquisition was repeated during a time period of 10 minutes in rapid succession (i.e. no delays) immediately after contrast administration, then was performed after a 3–5 min delay from the end of the first acquisition, imaging at 2 minutes interval. All contrast-enhanced imaging was performed with the same T1-weighted sequence optimized before contrast injection. Unenhanced and contrast-enhanced MRI examinations were performed in the sagittal plane, with a temporal resolution varying between 45 sec to 70 sec per volume with an approximate total imaging time of 30–35 min per examination. Number of slices varied depending on the size of the breast.

Due to the fact that high spatial resolution was required for these scans (they were also used for diagnostic purposes), the temporal resolution was not considered adequate for a two-compartment Tofts-based pharmacokinetic analysis. Therefore, to extract dynamic parameters with potential prognostic value, we fitted the image intensity data, pixel by pixel, to an empiric function with exponential increase and exponential decrease, as first proposed by Kurland et al. (30),:

$$S_p(t) = S_{max}\left[1 - e^{-Wi(t-t_0)}\right] e^{-Wo(t-t_0)} \quad (1)$$

where S_p is the percent change in image intensity enhancement $S_p = (I_{post} - I_{pre})/ I_{pre} \times 100$, S_{max} is the maximum image enhancement, W_i is the rate of contrast washin, W_o is the rate of contrast washout, t_0 is the time at the beginning of the Gd injection, and $t\text{-}t_0$ is the time after injection. To account for both the velocity and magnitude of enhancement we defined a washin parameter (WiP) as the slope of the above function at $t = t_0$, i.e. $WiP = S_{max} \times Wi$, also known as relative perfusion index (30). The WiP is thought to be a surrogate for the tumor's vascularity/permeability (31). We call the images created using this parameter WiP maps, and we use them as surrogate images for the tumor's vascularity/permeability. The WiP maps are a result of the transport of Gd-DTPA into the interstitial space. This transport can either be due to convection or diffusion. To exclude the latter, a minimum WiP value was set for inclusion in the analysis, by estimating the times it takes a Gd-DTPA molecule to move across a pixel given its diffusion length scale. The minimum value of the WiP was set at 1% of the maximum value. Hence, all pixels with a WiP value less then the minimum value were not fitted ("no flow"), the others were fitted ("with flow") (32). Given that the CA preferentially accumulates in tumor, the WiP maps carry also morphologic information.

In generating the parametric maps we noticed two main types of enhancement, as previously described in the MR radiology literature: centripetal (CP) (9), characterized by inhomogeneous ring enhancement, and centrifugal (CF), characterized by a more homogenous enhancement from center to periphery.

We also defined a washout parameter (WoP) using the maximum signal intensity and the signal intensity ten minutes after CA injection, as $WoP = ABS[(I_{10}\text{-}I_{max})/(T_{10}\text{-}T_{max})]$ (see Figure 1C).

In order to extract different parameters with relevance in predicting response, image intensity data were fitted, pixel by pixel, to the empiric exponential function from equation (1). The analysis was then carried out on regions of interest (ROI). An optimal method for ROI depiction is not established. DCE-MRI breast imaging literature recommends the use of an ROI comprised of the most enhancing pixels (9, 10, 12, 16). Subsequently, we have elected to depict the ROIs on the WiP maps at the central plane of the tumor. This area was interrogated by computer code to select a 16 (4 × 4) pixel region (varying in size depending on the FOV from 12 to 16 mm^2) showing the greatest mean maximum percent enhancement. This particular size was selected to mitigate between not selecting the most enhancing pixels that might be outliers, and avoiding partial volume averaging.

The CA enhancement curve analysis was performed for each patient considered, and WiP maps were generated, together with values for WiP and WoP in the selected ROIs. The extracted MR parameters were not individually correlated with response. Alternately, these three variables were combined into a Morpho-Physiological Tumor Score (MPTS) with the intent of achieving more robust prognostic efficacy.

In deriving the MPTS score we had three working hypothesis that link the MR derived parameters to response:

1. Inhomogeneous ring enhancement, as indicated by the centripetal morphology, may reflect increases in the treatment resistance. If the enhancement correlates with drug delivery, this type of pattern would possibly reflect inhomogeneity in drug delivery.
2. Increased vascularity/permeability, as indicated by increased WiP, increases the resistance to treatment, secondary to increased altered, abnormal vascularity.
3. Decreased extravascular extracellular space, as indicated by increased WoP, increases the resistance to treatment, secondary to decreased drug delivery.

The novel MPTS has three components: the first component of the score is related to morphology and comes from the shape of the parametric WiP maps. As the morphological component of the MPTS, a tumor was given a score of 2 if the enhancement pattern is centrifugal (CF), and 0 if centripetal (CP).

The second and third components are physiological (one related to the tumor vascularity/permeability and the other to tumor extracellular extravascular space) defined by the WiP and WoP. The ranges for the WiP and WoP were determined empirically on a learning set of five patients treated earlier on the Phase I portion of this protocol, and applied prospectively on 20 other patients. For scoring purposes, the ranges for WiP and WoP were established as follows: score of 2 for WiP < 100, 1 for 100 <= WiP < 200, and 0 for 200 <= WiP. For WoP: score of 2 for WoP < 1, 1 for 1 <= WoP < 2, and 0 for 2 <= WoP.

The final MPTS was determined by adding the score from the three components. The MPTS scores were finally divided in ranges to predict for possible complete responders (MPTS = 6), partial responders (MPTS = 2 to 5), and non responders (MPTS = 0 to 1). Table 1 summarizes the three components of the MPTS with the convention used for scoring.

The response based on the MPTS was compared to the pathological response determined from the residual tumor as quantified from the largest linear dimension (pathology size vs. pre cycle I DCE-MRI size). Complete pathological response was defined by absence of disease in the breast and axilla. Pathological partial response was defined as more than 50% reduction in tumor size when pre-treatment MR size was compared to post treatment surgery size. For less then 50 % reduction, the patients were considered pathological non-responders.

2.4 Statistical Methods

There are two angles to look at this prediction problem statistically: 1) One is from a diagnostic perspective. That is, we would like to see a very high utility of predicting treatment response based on the MPTS score using as reference the actual pathological response. Sensitivity, specificity and related odds ratio are used in this setting. 2) The other is from an agreement perspective. Here we would like to see a very high agreement between the predicted response and the actual pathological response. The Kappa statistic was used with respect to this approach using SAS software (SAS Institute Inc., Cary, NC)

3. Results

Forty-four patients were enrolled on this PhaseI/II trial. However, a 20-patient subgroup from Phase II was used for this study (median age = 46.5 ± 10.3 yrs.). These particular patients were chosen from the whole group because the MR data was acquired using the same protocol, and because the patients were all at the same Paclitaxel and liposomal doxorubicin dosage.

All the patients included in this study completed all four prescribed HT cycles. The total time at power on averaged over the 20 patients was 238 ± 23 min, 247 ± 2.4 min for responders, and 227 ± 30 min for non-responders. Two of the nine non-responders had less then 180 total minutes at power on. The average CEM43T90 for all 20 patients was 33 ± 45.6 min, with 50 ± 55 min for responders, and 12 ± 16 min for non-responders. Four of the nine non-responders, or 44%, and three of the eleven responders, or 27 %, had an averaged CEM43T90 less then 10 minutes, valued proved by two randomized trials to improve tumor response and duration of local control (33,34).

Figure 3 shows two sequences of DCE-MR images before and after bolus injection of Gd-DTPA contrast for a patient with centrifugal enhancement (A), and centripetal enhancement (B). These images alone cannot differentiate between a CF and CP morphology. Figure 4

shows, for the same two patients from Figure 3, FSE images (A1, A2), subtraction images (B1, B2) between the maximum enhancement and baseline, and WiP maps (C1, C2). One can notice that only the WiP map is able to differentiate between a centrifugal and a centripetal morphology for the second case.

Figure 5 exemplifies the two types of enhancement encountered in LABC patients: centrifugal (CF) and centripetal (CP). From these images one can also see the advantage of a WiP map over the raw DCE-MRI images in pinpointing areas of tumor inhomogeneity. Six out of 20 lesions (30%) had a CF enhancement pattern, the remaining 14/20 (70%) a CP pattern.

The WiP and WoP varied significantly for different tumors: WiP varied from 52 to 266, and the WoP from 0.6 to 8.5. For the washin characteristics, 7/20 patients (35%) had a WiP value < 100 (score of 2), 8/20 patients (40%) had a 100 <= WiP < 200 (score of 1), and the remaining 5/20 patients (25%) had a WiP >= 200 (score of 0). For the washout characteristics, 3/20 patients (15%) had a WoP < 1 (score of 2), 7/20 (35 %) had 1 <= WoP < 2 (score of 1), and 10/20 patients (50 %) had WiP >= 2 (score of 0).

Figures 6A and B show examples of the MPTS derivation for a responder and non-responder, respectively. The enhancement curve is depicted with the parametric map as an insert. The enhancement pattern score, and the WiP and WoP values and scores are listed together with the overall MPTS for both patients. The difference in the magnitude of early and late enhancement between the two patients is easily distinguishable with the non-responder exhibiting increased vascularity/permeability, as indicated by increased WiP (209 vs. 68.4 for the responder), that translates, per our hypothesis, in resistance to treatment. Also, the non-responding tumor exhibits decreased extracellular extravascular space, as indicated by increased WoP (8.5 vs. 0.6 for the responder), that also increases the resistance to treatment, secondary to decreased drug delivery. The CEM43T90 achieved for these two patients was similar, 14.4 min for the CR, and 13.6 for the NR.

Table 2 summarizes the maximum size per pretheraphy DCE-MRI, the post treatment largest diameter per pathology, the MR extracted parameters (enhancement pattern, WiP and WoP) with the associate score, and the overall MPTS derived for each patient. The CEM43T90, the predicted response based on the MPTS and the pathological response were also listed.

Of the patients with a score in the 2–6 range, 10/12 (83%), with a 95% confidence interval (CI) of 52%–98%, were responders. Of the patients with a score between 0 and 1, 1/8 (13%), with a 95% CI of 0.3%–53% were responders. The sensitivity for predicting response with MPTS is 91% while the specificity is 78%, when using as the gold standard the actual treatment response based on the residual tumor as quantified from the largest linear dimension (pathology size vs. pre cycle I MR size). The overall misclassification rate by MPTS is 15% (3/20). The odds ratio of responding to treatment between the high (2–6) MPTS and low (0–1) MPTS groups is 35 ($p<0.05$), implying that the MPTS score is highly predictive of the pathological response. The kappa statistic gave a value of 0.69 with a 95% CI of [0.38, 1.00] and $p=0.002$, indicating a very high agreement between the predicted response and the actual pathological response.

4. Discussion

Despite recent advances in combined multimodality treatments, locally advanced breast carcinoma continues to carry a poor prognosis. Since neoadjuvant therapies are receiving increased attention for management of LABC, tools to predict and monitor tumor response are needed. Improved diagnostic and therapy monitoring in breast requires moving beyond anatomical images. Early and reliable assessment of functional properties of lesions has become a necessity to correctly: diagnose, differentiate and guide therapy. Functional imaging,

i.e. the imaging of metabolism, perfusion and diffusion is of active interest. Changes in metabolism and perfusion occur before morphological changes, and the pretherapeutic values of these physiological parameters have the potential to characterize the way a certain tumor will respond to treatment.

The neoadjuvant regimen used in this study was Paclitaxel (Taxol, Bristol-Myers Squibb, Prinston, NJ), liposomal doxorubicin (Myocet, Elan Pharmaceuticals, Princeton, NJ) and HT every 21 days, for a total of four cycles. Liposomal chemotherapeutic agents were designed to increase the amount of drug delivered to tumors and decrease the amount going to healthy organs. Using hyperthermia to target drug release is a novel approach.

The purpose of this study was to define a morpho-physiological tumor score that will synergistically combine several DCE-MRI parameters that can be prospectively used to determine if a particular tumor will respond to a combination of neoadjuvant chemotherapy and hyperthermia.

Our study shows that combining information about the tumor enhancement pattern (morphology information) with information extracted from a semi-quantitative analysis of the time/intensity curves of the contrast agent, WiP, WoP (physiological information), a Morpho-Physiological Tumor Score can be defined that was shown to predict with a sensitivity of 91%, and a specificity of 78 % if a tumor will respond to treatment, when compared to actual treatment response based on residual tumor size (pathology size vs. pre cycle I MR size).

All 20 patients included in this treatment completed all four prescribed HT cycles. The thermal metric reported here, the CEM43T90 was on average larger for responders, then for non-responders (50 min vs. 12 min.). Of the seven patients receiving suboptimal HT treatments, i.e. CEM43T90 <10 min, four were non-responders, and three were responders. However, these 7/20 patients had a WiP > 127, in agreement with one of our hypothesis that increased vascularity/permeability, as indicated by increased WiP, increases the resistance to treatment, secondary to increased altered, abnormal\vascularity. Interestingly, 2/3 responders with CEM43T90 < 10 min had CP enhancement that, we hypothesize, helped deliver the drug more uniformly.

One possible limitation of the study is that, as described earlier, the ranges for the WiP and WoP were determined from previous work on a set of 5 patients that underwent the same type of therapy on the early stage of the Phase I portion of the trial and were then applied prospectively to the 20 patients reported on here. Consequently, these values cannot be generalized to other trials, rather taken as parameters that have to be determined for each neo-adjuvant therapy used.

Another possible limitation of this study is related to the method used to extract the MR parameters (the analysis of the time/intensity curves based on a simple double exponential fit). Semi-quantitative methods used to characterize the time/intensity curves are reported to suffer from lack of reproducibility and to be reader dependent (35), (18). To understand the need for this approach we will revisit the spatial-temporal resolution dilemma in dynamic MRI. The requirements for temporal and spatial resolution for breast, or any oncology application, are generally in conflict (36). As reported by Kuhl et al. (37), when the scans are used for diagnostic purpose (differentiate between benign and malignant breast lesions), increased spatial resolution significantly improves diagnostic confidence and accuracy of dynamic MRI, even if this improvement occurs at the expense of temporal resolution. They also note that loss of kinetic information regarding enhancement rates is not diagnostically relevant. However, when DCE-MRI is used to characterize contrast kinetics, high temporal resolution is crucial for sampling the changes in the blood contrast agent concentration as a function of time. The temporal requirements for sampling this concentration have been considered in detail by

Henderson et al. (38) and summarized by Evelhoch (36). They recommend temporal sampling less then 16 sec for the errors in the estimation of the kinetic parameters to be low. Hence, due to the fact that our scans were taken at temporal resolution of 45–70 seconds, temporal resolution was deemed unsatisfactory for any meaningful pharmacokinetic analysis. Another limitation is the use of parameters in the scoring system based on maximum signal intensity that can be scanner dependent. That might result in the impossibility of applying the threshold values described here (see Table 1) to other studies performed on different scanners.

The division of enhancement patterns into just two categories, homogeneous (CP) and enhancing rim (CF), may seem somewhat arbitrary, when the Breast Imaging-Reporting and Data System BI-RADS (39) for MRI classification for breast include: homogeneous, heterogeneous, rim enhancement, dark internal septation, enhancing internal septation, and central enhancement . Although most of these patterns were encountered in the study, the classification we picked was based on our hypothesis that an inhomogeneous ring enhancement, as indicated by the centripetal morphology, increases the resistance to treatment, secondary to decreased and inhomogeneous drug delivery, as opposed to all the other patterns that might indicate an environment conducive to better drug delivery.

5. Conclusion

Our study shows that pre-treatment MR-extracted parameters such as enhancement pattern, washin and washout parameters can be combined into a Morpho-Physiological Tumor Score that correlates well with pathological response in LABC patients treated with neoadjuvant chemotherapy and hyperthermia.

Although this is a pilot study involving a limited number of patients, it provides evidence that the MPTS derived from contrast agent-enhancement analysis of pre-treatment MRI images has the potential to predict response to neoadjuvant chemotherapy and hyperthermia in locally advanced breast cancer patients. Further larger prospective studies are needed to confirm the validity of these results.

Statement of Clinical Relevance

Combined therapies represent a staple of modern medicine. For women treated with neoadjuvant chemotherapy (NA ChT) for locally advanced breast cancer (LABC), early determination of whether the patient will fail to respond can enable the use of alternative, more beneficial therapies. This is even more a desiderate when the combined therapy includes hyperthermia (HT), an efficient way to improve drug delivery, however more costly and time consuming. There is data showing that this goal can be achieved using magnetic resonance imaging (MRI) with contrast agent (CA) enhancement. This work proposes for the first time combining the information extracted from pretreatment MR imaging into a Morpho-Physiological Tumor Score (MPTS) with the hypothesis that this score will increase the prognostic efficacy, compared to each of its MR-derived components: morphological (derived from the shape of the tumor enhancement) and physiological (derived from the CA enhancement variance dynamics parameters). The MPTS was correlated with response as determined by both pathologic residual tumor and MRI imaging and was shown that it has potential to predict response. The MPTS was extracted from pretreatment MRI parameters, so independent of the combined therapy used. Further larger prospective studies are needed to confirm the validity of these results.

Acknowledgments

This work was supported by a grant from the NCI CA42745, Dewhirst MW – PI.

REFERENCES

1. Hortobagyi, GN.; Singletary, SE.; McNeese, MD. Treatment of locally advanced and inflammatory breast cancer. In: Harris, J., editor. Breast Diseases. 1996. p. 585-599.
2. Hortobagyi GN, Buzdar AU. Management of locally advanced breast cancer. Am J Clin Oncol 1988 Oct;11(5):597–601. [PubMed: 2845771]
3. Pickles MD, Lowry M, Manton DJ, Gibbs P, Turnbull LW. Role of dynamic contrast enhanced MRI in monitoring early response of locally advanced breast cancer to neoadjuvant chemotherapy. Breast Cancer Res Treat 2005 May;91(1):1–10. [PubMed: 15868426]
4. Abraham DC, Jones RC, Jones SE, Cheek JH, Peters GN, Knox SM, et al. Evaluation of neoadjuvant chemotherapeutic response of locally advanced breast cancer by magnetic resonance imaging. Cancer 1996 Jul 1;78(1):91–100. [PubMed: 8646731]
5. Robinson SP, Howe FA, Rodrigues LM, Stubbs M, Griffiths JR. Magnetic resonance imaging techniques for monitoring changes in tumor oxygenation and blood flow. Semin Radiat Oncol 1998 Jul;8(3):197–207. [PubMed: 9634496]
6. Hylton NM. Vascularity assessment of breast lesions with gadolinium-enhanced MR imaging. Magn Reson Imaging Clin N Am 2001 May;9(2):321–332. vi. [PubMed: 11493422]
7. Knopp MV, Weiss E, Sinn HP, Mattern J, Junkermann H, Radeleff J, et al. Pathophysiologic basis of contrast enhancement in breast tumors. J Magn Reson Imaging 1999 Sep;10(3):260–266. [PubMed: 10508285]
8. Knopp MV, von Tengg-Kobligk H, Choyke PL. Functional magnetic resonance imaging in oncology for diagnosis and therapy monitoring. Mol Cancer Ther 2003 Apr;2(4):419–426. [PubMed: 12700286]
9. Helbich TH. Contrast-enhanced magnetic resonance imaging of the breast. Eur J Radiol 2000 Jun;34 (3):208–219. [PubMed: 10927162]
10. Schnall MD. An overview of interpretation strategies for breast MR imaging. Magn Reson Imaging Clin N Am 2001 May;9(2):289–294. v–vi. [PubMed: 11493419]
11. Schnall M, Orel S, Breast MR. imaging in the diagnostic setting. Magn Reson Imaging Clin Am 2006 Aug;14(3):329–337. vi.
12. Kuhl CK, Mielcareck P, Klaschik S, Leutner C, Wardelmann E, Gieseke J, et al. Dynamic breast MR imaging: are signal intensity time course data useful for differential diagnosis of enhancing lesions? Radiology 1999 Apr;211(1):101–110. [PubMed: 10189459]
13. Kuhl CK, Schild HH. Dynamic image interpretation of MRI of the breast. J Magn Reson Imaging 2000 Dec;12(6):965–974. [PubMed: 11105038]
14. Daniel BL, Yen YF, Glover GH, Ikeda DM, Birdwell RL, Sawyer-Glover AM, et al. Breast disease: dynamic spiral MR imaging. Radiology 1998 Nov;209(2):499–509. [PubMed: 9807580]
15. Flickinger FW, Allison JD, Sherry RM, Wright JC. Differentiation of benign from malignant breast masses by time-intensity evaluation of contrast enhanced MRI. Magn Reson Imaging 1993;11(5): 617–620. [PubMed: 8345775]
16. Liney GP, Gibbs P, Hayes C, Leach MO, Turnbull LW. Dynamic contrast-enhanced MRI in the differentiation of breast tumors: user-defined versus semi-automated region-of-interest analysis. J Magn Reson Imaging 1999 Dec;10(6):945–949. [PubMed: 10581507]
17. Tofts PS, Kermode AG. Measurement of the blood-brain barrier permeability and leakage space using dynamic MR imaging. 1. Fundamental concepts. Magn Reson Med 1991 Feb;17(2):357–367. [PubMed: 2062210]
18. Martincich L, Montemurro F, De Rosa G, Marra V, Ponzone R, Cirillo S, et al. Monitoring response to primary chemotherapy in breast cancer using dynamic contrast-enhanced magnetic resonance imaging. Breast Cancer Res Treat 2004 Jan;83(1):67–76. [PubMed: 14997056]
19. Julius T, Kemp SE, Kneeshaw PJ, Chaturvedi A, Drew PJ, Turnbull LW. MRI and conservative treatment of locally advanced breast cancer. Eur J Surg Oncol 2005 Dec;31(10):1129–1134. [PubMed: 15905068]
20. Wasser K, Klein SK, Fink C, Junkermann H, Sinn HP, Zuna I, et al. Evaluation of neoadjuvant chemotherapeutic response of breast cancer using dynamic MRI with high temporal resolution. Eur Radiol 2003 Jan;13(1):80–87. [PubMed: 12541113]

21. Delille JP, Slanetz PJ, Yeh ED, Halpern EF, Kopans DB, Garrido L. Invasive ductal breast carcinoma response to neoadjuvant chemotherapy: noninvasive monitoring with functional MR imaging pilot study. Radiology 2003 Jul;228(1):63–69. [PubMed: 12775851]
22. Drew PJ, Kerin MJ, Mahapatra T, Malone C, Monson JR, Turnbull LW, et al. Evaluation of response to neoadjuvant chemoradiotherapy for locally advanced breast cancer with dynamic contrast-enhanced MRI of the breast. Eur J Surg Oncol 2001 Nov;27(7):617–620. [PubMed: 11669587]
23. Szabo BK, Aspelin P, Kristoffersen Wiberg M, Tot T, Bone B. Invasive breast cancer: correlation of dynamic MR features with prognostic factors. Eur Radiol 2003 Nov;13(11):2425–2435. [PubMed: 12898176]
24. Chang YC, Huang CS, Liu YJ, Chen JH, Lu YS, Tseng WY. Angiogenic response of locally advanced breast cancer to neoadjuvant chemotherapy evaluated with parametric histogram from dynamic contrast-enhanced MRI. Phys Med Biol 2004 Aug 21;49(16):3593–3602. [PubMed: 15446790]
25. Wedam SB, Low JA, Yang SX, Chow CK, Choyke P, Danforth D, et al. Antiangiogenic and antitumor effects of bevacizumab in patients with inflammatory and locally advanced breast cancer. J Clin Oncol 2006 Feb 10;24(5):769–777. [PubMed: 16391297]
26. Padhani AR, Hayes C, Assersohn L, Powles T, Makris A, Suckling J, et al. Prediction of clinicopathologic response of breast cancer to primary chemotherapy at contrast-enhanced MR imaging: initial clinical results. Radiology 2006 May;239(2):361–374. [PubMed: 16543585]
27. Manton DJ, Chaturvedi A, Hubbard A, Lind MJ, Lowry M, Maraveyas A, et al. Neoadjuvant chemotherapy in breast cancer: early response prediction with quantitative MR imaging and spectroscopy. Br J Cancer 2006 Feb 13;94(3):427–435. [PubMed: 16465174]
28. Wu L, McGough RJ, Arabe OA, Samulski TV. An RF phased array applicator designed for hyperthermia breast cancer treatments. Phys Med Biol 2006 Jan 7;51(1):1–20. [PubMed: 16357427]
29. Sapareto SA, Dewey WC. Thermal dose determination in cancer therapy. Int J Radiat Oncol Biol Phys 1984 Jun;10(6):787–800. [PubMed: 6547421]
30. Kurland RJ, Shoop JD, Funkhouser GR. A Kinetic Model for Time Development of Gd-DTPA in Relaxation Enhancement (Abstr.). Magn Reson Imag 1989;7:177.
31. Belfi CA, Paul CR, Shan S, Ngo FQ. Comparison of the effects of hydralazine on tumor and normal tissue blood perfusion by MRI. Int J Radiat Oncol Biol Phys 1994 Jun 15;29(3):473–479. [PubMed: 8005802]
32. Craciunescu OI, Das SK, McCauley RL, MacFall JR, Samulski TV. 3D numerical reconstruction of the hyperthermia induced temperature distribution in human sarcomas using DE-MRI measured tissue perfusion: validation against non-invasive MR temperature measurements. Int J Hyperthermia 2001 May–Jun;17(3):221–239. [PubMed: 11347728]
33. Jones EL, Oleson JR, Prosnitz LR, Samulski TV, Vujaskovic Z, Yu D, et al. Randomized trial of hyperthermia and radiation for superficial tumors. J Clin Oncol 2005 May 1;23(13):3079–3085. [PubMed: 15860867]
34. Thrall DE, LaRue SM, Yu D, Samulski T, Sanders L, Case B, et al. Thermal dose is related to duration of local control in canine sarcomas treated with thermoradiotherapy. Clin Cancer Res 2005 Jul 15;11(14):5206–5214. [PubMed: 16033838]
35. Taylor JS, Reddick WE. Evolution from empirical dynamic contrast-enhanced magnetic resonance imaging to pharmacokinetic MRI. Adv Drug Deliv Rev 2000 Mar 15;41(1):91–110. [PubMed: 10699307]
36. Evelhoch JL. Key factors in the acquisition of contrast kinetic data for oncology. J Magn Reson Imaging 1999 Sep;10(3):254–259. [PubMed: 10508284]
37. Kuhl CK, Schild HH, Morakkabati N. Dynamic bilateral contrast-enhanced MR imaging of the breast: trade-off between spatial and temporal resolution. Radiology 2005 Sep;236(3):789–800. [PubMed: 16118161]
38. Henderson E, Rutt BK, Lee TY. Temporal sampling requirements for the tracer kinetics modeling of breast disease. Magn Reson Imaging 1998 Nov;16(9):1057–1073. [PubMed: 9839990]
39. Ikeda DM, Hylton NM, Kinkel K, Hochman MG, Kuhl CK, Kaiser WA, et al. Development, standardization, and testing of a lexicon for reporting contrast-enhanced breast magnetic resonance imaging studies. J Magn Reson Imaging 2001 Jun;13(6):889–895. [PubMed: 11382949]

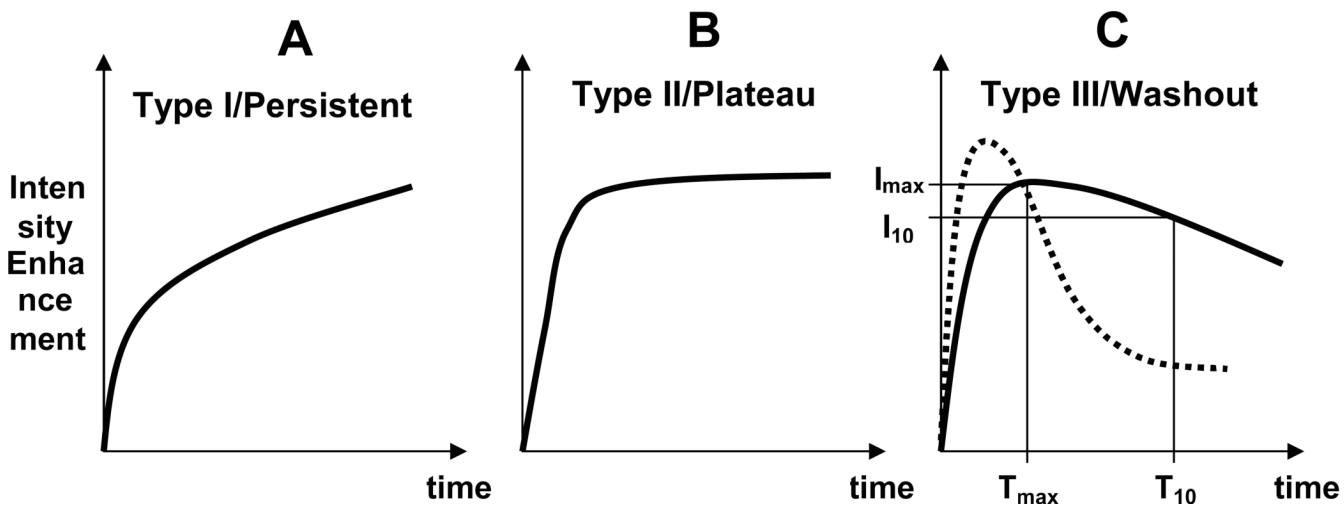

Figure 1.

Graphs depicting three patterns of enhancement curves typically seen in breast lesions, as intensity enhancement as a function of time. A) type I – "persistent enhancing", B) type II – "plateau" and C) type III –"washout", with two different trends(solid and dotted line) both of which are encountered in LABC patients. The slope of the late enhancement (or washout) can be described with the washout parameter: WoP = ABS[(I_{10}-I_{max})/(T_{10}-T_{max})] (see text).

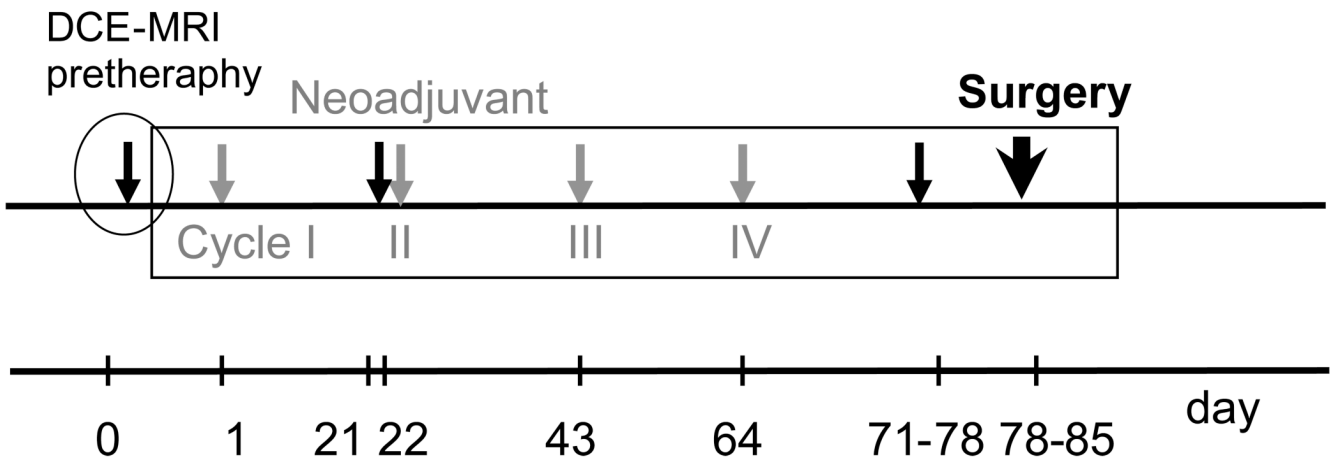

Figure 2.

Neoadjuvant PhaseI/II Trial Schema that was used at our Institution for LABC patients between 2000 and 2004. The schema consisted of 4 cycles of Paclitaxel, Liposomal Doxorubicin and HT (grey arrows) followed by surgery (bold arrow), with three dedicated MRI sessions (filled arrows) scheduled pre cycle I, II and pre surgery. The pretherapy DCE-MRI set used in this study is circled on the time line.

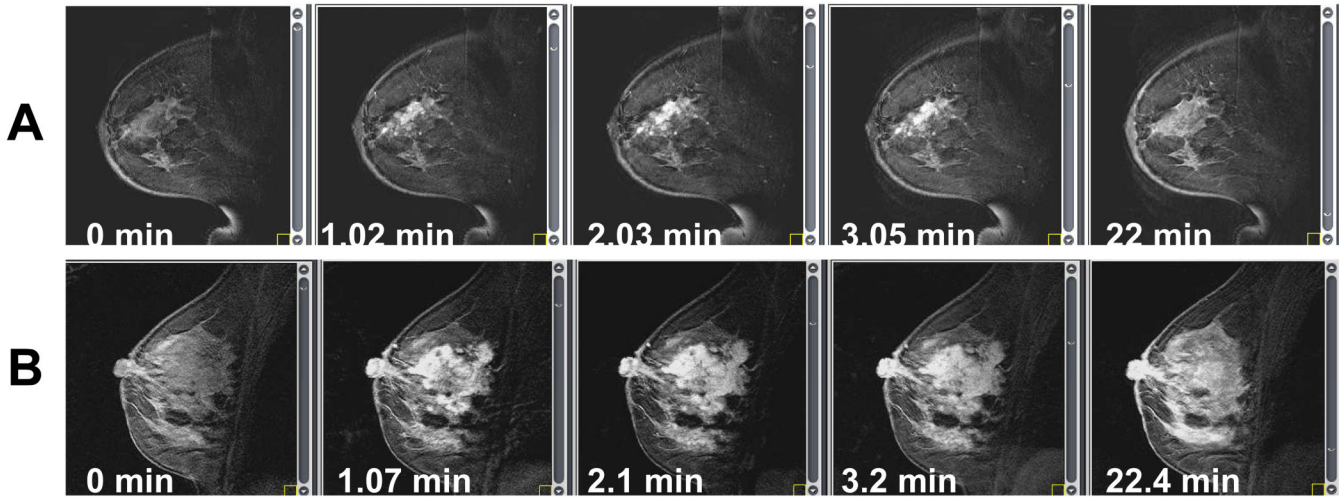

Figure 3.
Sequence of DCE-MRI images taken before (time t = 0 min)) and after bolus injection of the contrast agent Gd-DTPA for two different patients: A) centrifugal enhancement, B) centripetal enhancement.

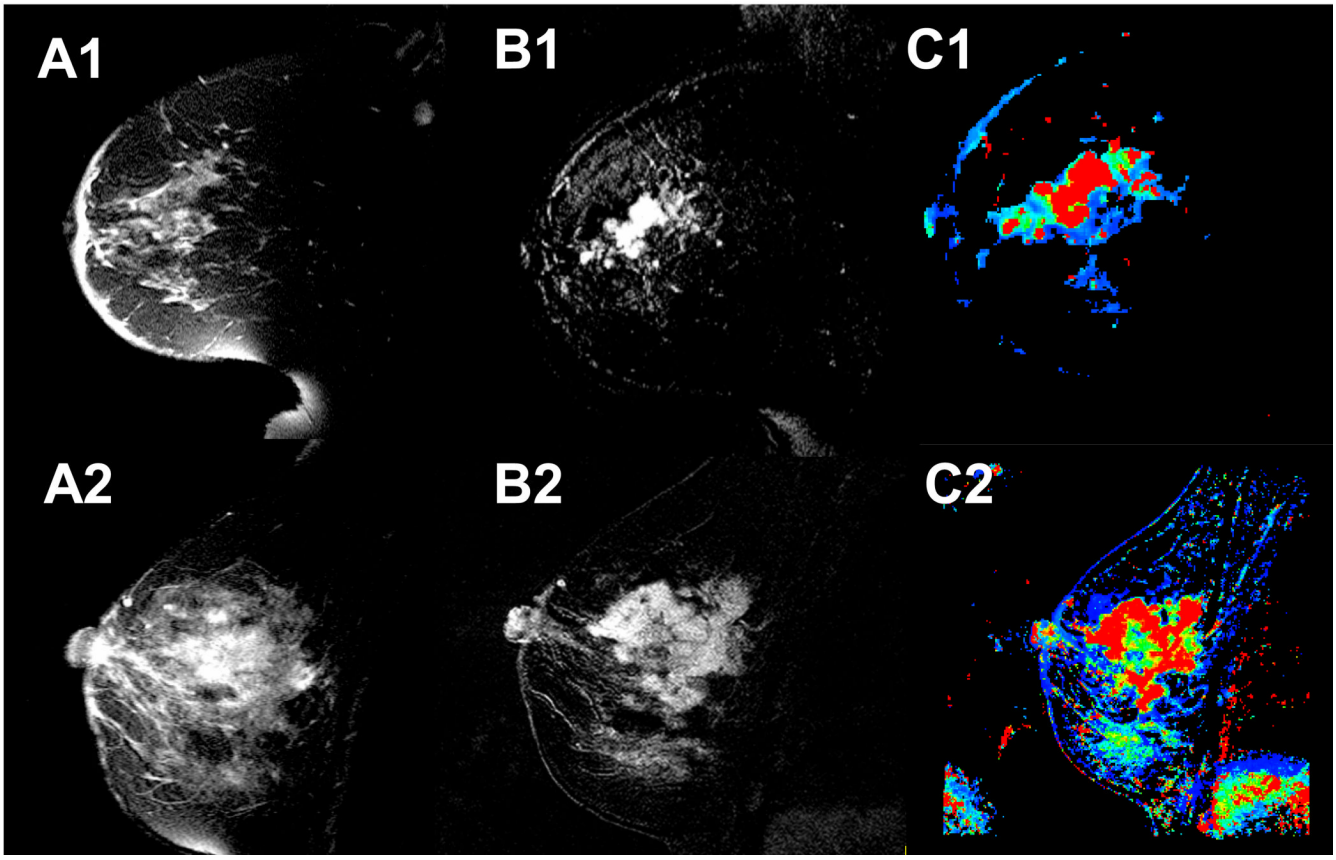

Figure 4.
For the same two patients from Figure 3, fast spin echo images (A1, A2), subtraction images between the maximum enhancement time point and baseline (B1, B2), and WiP maps (C1, C2).

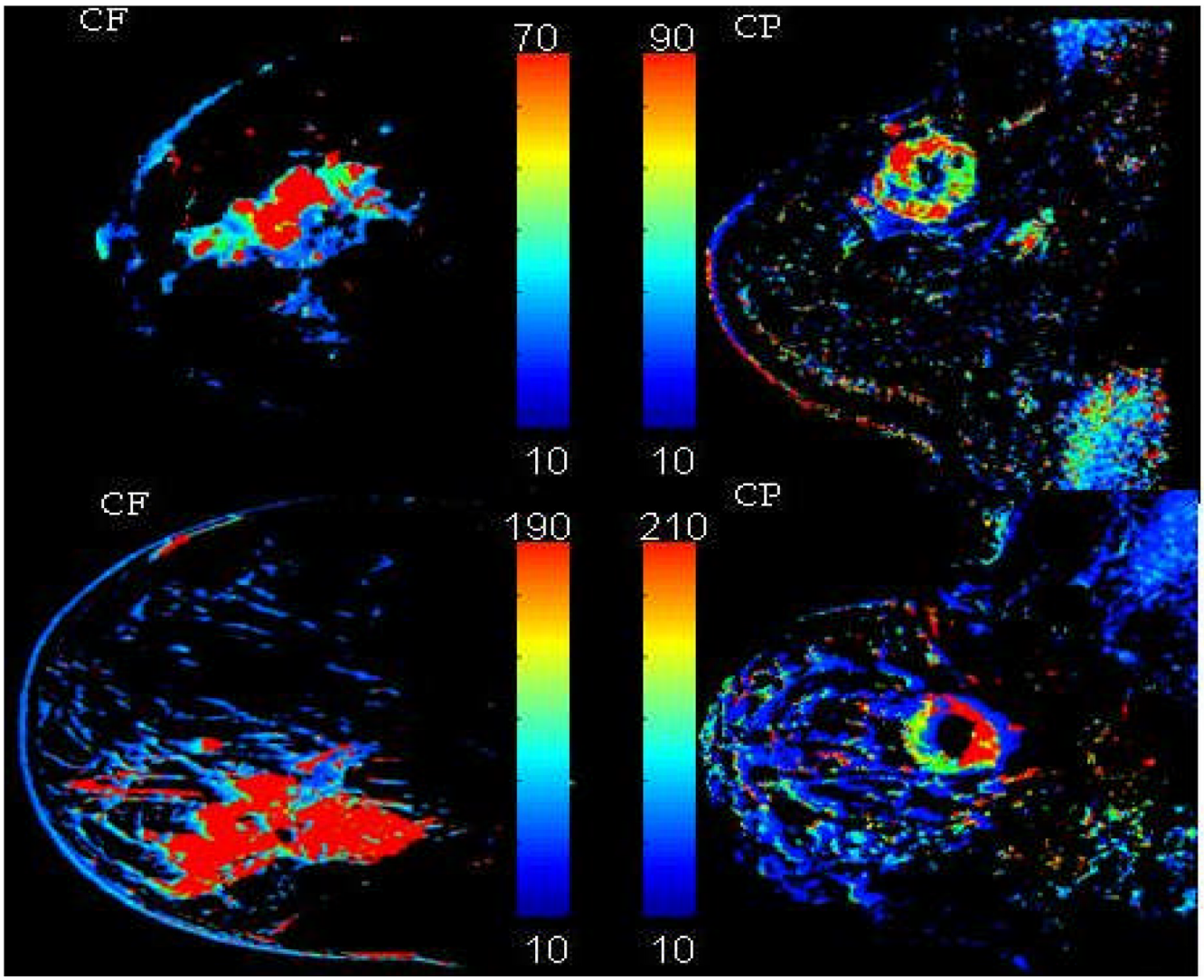

Figure 5.
WiP maps generated from DCE-MRI that exemplify the type of enhancement noted in LABC patients: left column, centrifugal (CF), uniform enhancement from center to periphery; right column, centripetal (CP), inhomogeneous ring-type enhancement.

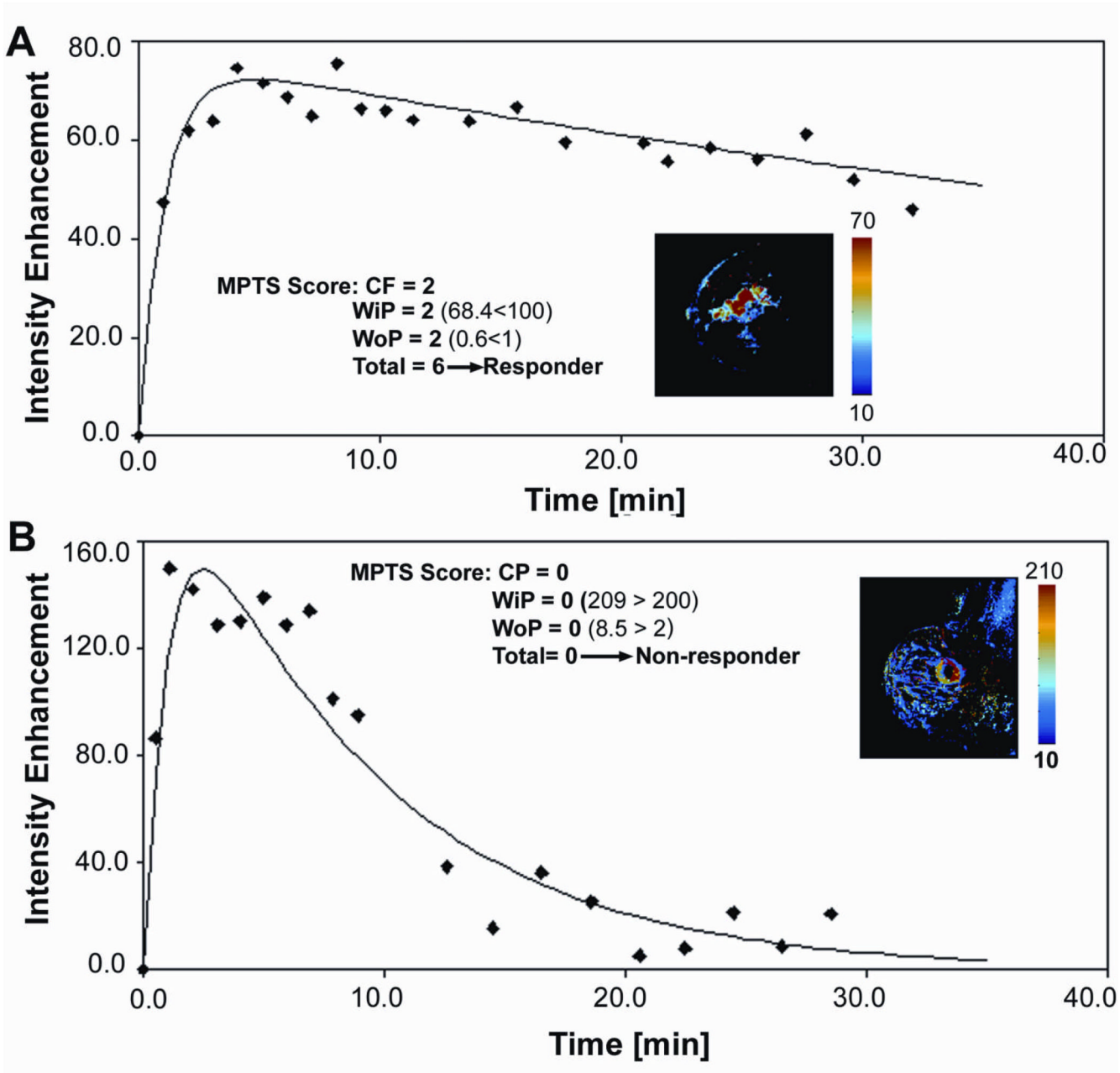

Figure 6.

A) Example of a 53 yr old patient (T_4dN_x at diagnosis) with a MPTS score of 6 who ultimately was a pathological complete responder (pT_0N_0). Shown here are the WiP parametric map with centrifugal morphology, and an enhancement curve with low WiP and WoP; B) Example of a 64 yr old patient (T2N1 at diagnosis) with an MPTS score of 0 who was ultimately a pathological non-responder (pT2N1). The WiP parametric map shows centripetal morphology, and the WiP and WoP are high.

Table 1

Components of the MPTS: The first component of the score is related to morphology and comes from the shape of the parametric maps. The second and third components are physiological defined by the WiP and WoP. The ranges for the WiP and WoP were determined empirically from previous work. The MPTS is the sum score of the three components.

Parameter	Score
Enhancement Pattern	
Centrifugal (CF)	2
Centripetal (CP)	0
WiP	
WiP < 100	2
100 <= WiP < 200	1
200 <= WiP	0
WoP	
WoP < 1	2
1 <= WoP < 2	1
2 <= WoP	0

Int J Hyperthermia. Author manuscript; available in PMC 2009 November 26.

Table 2

Maximum diameter per pretherapy DCE-MRI in cm, post treatment (TX) largest dimension per pathology in cm, MR extracted parameters, enhancement pattern, WiP and WoP and the corresponding score, and the overall MPTS derived for each patient. The CEM43T90 and both predicted response based on the MPTS and the actual pathological response are also listed. Patients are sorted by the MPTS score from highest to lowest.

No.	Maximum Diameter Per Pretheraphy DCE-MRI [cm]	Post TX Largest Dimension Per Pathology [cm]	CEM43T 90 [min.]	Enhancement Pattern (Score)	WiP [−] (Score)	WoP [−] (Score)	MPTS	Predicted Response	Pathological Response
1	8.0	NRC	14.5	CF(2)	68.4 (2)	0.6 (2)	6	CR	CR
2	8.0	1.0	50.6	CF(2)	84.8 (2)	1.0 (1)	5	PR	PR
3	9.0	NRC***	150.7	CF(2)	97.0 (2)	1. 8(1)	5	PR	PR
4	11.0	0.9	6.9	CF(2)	188.2 (1)	1.6 (1)	4	PR	PR
5	6.0	3.0	32.5	CP(0)	47.1 (2)	0.9 (2)	4	PR	PR
6	11.0	5.0	9.1	CF(2)	142.1 (1)	3.0 (0)	3	PR	PR
7	2.5	2.3	12.3	CP(0)	67.6 (2)	1.1 (1)	3	*PR**	NR
8	6.0	3.7	10.9	CP(0)	61.0 (2)	1.1 (1)	3	PR	PR
9	6.4	5.7	13.7	CP(0)	24.6 (2)	2.6 (0)	2	*PR**	NR
10	7.3	2.5	8.7	CP(0)	210.1 (0)	0.0 (2)	2	PR	PR
11	6.1	2.2	60.2	CP(0)	196.7(1)	1.1 (1)	2	PR	PR
12	10.0	1.8	44.7	CF(2)	298.3 (0)	5.0 (0)	2	PR	PR
13	4.0	3.7	1.5	CP(0)	187.9 (1)	2.0 (0)	1	NR	NR
14	2.9	3.0	52.5	CP(0)	142.1 (1)	3.2 (0)	1	NR	NR
15	3.6	2	11.8	CP(0)	162.5 (1)	2.8 (0)	1	NR	NR
16	9.4	7.5	2.5	CP(0)	266.3 (0)	1.4 (1)	1	NR	NR
17	8.0	1.5	159.0	CP(0)	111.4 (1)	8.3 (0)	1	*NR***	PR
18	6.0	8.0	0.8	CP(0)	127.0 (1)	5.3 (0)	1	NR	NR
19	3.0	2.0	13.6	CP(0)	209.0 (0)	8.5 (0)	0	NR	NR
20	6.0	7.5	2.6	CP(0)	250.0(0)	10.5 (0)	0	NR	NR

* false positive

** false negative

NRC = no residual carcinoma

*** positive axillary lymph nodes

Table 3

Summary of MPTS for the 20 patients evaluated in this study. Of the patients with a score in the 2–6 range, 10 (83%, 95% CI: 52%–98%) of 12 were responders. Of the patients with a score between 0 and 1, 1 (13%, 95% CI: 0.3%–53%) of 8 was responders.

MPTS	Pathological (p) Responders pCR+pPR	Pathological Non-Responders pNR	Total
2–6 Predicted Reponders	10	2	12
0–1 Predicted Non-responders	1	7	8
Total	11	9	20